Measurement of the helicity dependence for the $\gamma p \to n\pi^+$ channel in the second resonance region

J. Ahrens,[7] S. Altieri,[11,12] J. R. M. Annand,[5] H.-J. Arends,[7] R. Beck,[7,*] C. Bradtke,[1] A. Braghieri,[11] N. d'Hose,[4] H. Dutz,[2] S. Goertz,[1] P. Grabmayr,[13] S. Hasegawa,[9] E. Heid,[7] H. Holvoet,[3] L. Van Hoorebeke,[3] N. Horikawa,[10] T. Iwata,[9] O. Jahn,[7] P. Jennewein,[7] S. Kamalov,[7,†] F. Klein,[2] R. Kondratiev,[8] M. Lang,[7,*] B. Lannoy,[3] V. Lisin,[8] M. Martinez-Fabregate,[7] J. C. McGeorge,[5] W. Meyer,[1] A. Panzeri,[11,12] P. Pedroni,[11,‡] T. Pinelli,[11,12] I. Preobrajenski,[7,8] G. Reicherz,[1] Ch. Rohlof,[2] G. Rosner,[5] M. Rost,[7] T. Rostomyan,[3,11] D. Ryckbosch,[3] M. Schumacher,[6] B. Seitz,[6,§] G. Tamas,[7] A. Thomas,[7] L. Tiator,[7] R. van de Vyver,[3] and F. Zapadtka[6]

(GDH- and A-2 Collaborations)

[1]*Insitut für Experimentalphysik, Ruhr-Universität Bochum, D-44801 Bochum, Germany*

[2]*Physikalisches Institut, Universität Bonn, D-53115 Bonn, Germany*

[3]*Subatomaire en Stralingsfysica, Universiteit Gent, B-9000 Gent, Belgium*

[4]*CEA Saclay, DSM/DAPNIA/SPhN, F-91191 Gif-sur-Yvette Cedex, France*

[5]*Department of Physics & Astronomy, University of Glasgow, Glasgow G12 8QQ, United Kingdom*

[6]*II. Physikalisches Institut, Universität Göttingen, D-37077 Göttingen, Germany*

[7]*Institut für Kernphysik, Universität Mainz, D-55099 Mainz, Germany*

[8]*INR, Academy of Science, Moscow, Russia*

[9]*Department of Physics, Nagoya University, Chikusa-ku, Nagoya, Japan*

[10]*CIRSE, Nagoya University, Chikusa-ku, Nagoya, Japan*

[11]*INFN, Sezione di Pavia, I-27100 Pavia, Italy*

[12]*Dipartimento di Fisica Nucleare e Teorica, Università di Pavia, I-27100 Pavia, Italy*

[13]*Physikalisches Institut, Universität Tübingen, D-72076, Tübingen, Germany*

(Received 24 January 2006; published 20 October 2006)

The helicity dependence of the $\gamma p \to n\pi^+$ reaction has been measured for the first time in the photon energy range from 450 to 790 MeV. The experiment, performed at the Mainz Microtron (MAMI), used a 4π-detector system, a circularly polarized, tagged photon beam, and a longitudinally polarized frozen-spin target. Although these polarized data are mainly sensitive to mechanisms involving the $D_{13}(1520)$ resonance, a cusp structure at the η production threshold can be clearly observed. These data are significantly different from the predictions of the existing multipole analyses and are used to determine the helicity amplitudes of the $D_{13}(1520)$ and $S_{11}(1535)$ resonances with improved accuracy.

DOI: 10.1103/PhysRevC.74.045204 PACS number(s): 13.60.Le, 14.20.Gk, 25.20.Lj

I. INTRODUCTION

Single pion photoproduction is presently one of the main sources of information on the long-range structure of the nucleon. Over a 30-year period, substantial experimental effort has gone toward measuring these reactions, and a series of partial wave analyses of these data has attempted to extract the properties of the nucleon resonances and their couplings to the electromagnetic field. Nevertheless, despite this large effort, our understanding is still fragmentary. Many properties of the observed states, e.g., coupling constants, branching ratios, and helicity amplitudes, are poorly known. Furthermore, several states predicted by the nucleon-structure models have yet to be observed with confidence. It is often not clear if nonobservation implies that the model is wrong or merely that the signal is lost in the noise from more strongly excited resonances. In particular, the strong overlap of states above the dominant $P_{33}(1232)$ means that no clear resonance structure in the excitation function is observed.

Recently, fresh impetus has been given to this field by technological developments in polarized beam and polarized target techniques, which have opened the door to previously unmeasurable single and double polarization observables. This broadening of scope is vital to the removal of ambiguities inherent to partial wave analyses performed up to now and allows the weaker, more poorly known electromagnetic multipoles to be accessed. This has been clearly demonstrated in the Δ resonance region, where both the beam asymmetry (accessed by using a linearly polarized photon beam and an unpolarized target) and the helicity dependence (accessed by using a circularly polarized photon beam and a longitudinally polarized target) of single pion photoproduction have been measured with high precision [1–4] in order to precisely determine the role of the small electric quadrupole component of the proton wave function in the $N \to \Delta$ transition.

In the second resonance region ($500 \lesssim E_\gamma \lesssim 900$ MeV), where several overlapping states are present, e.g., $P_{11}(1440)$, $D_{13}(1520)$, and $S_{11}(1535)$, the helicity dependent observables

*Present address: Helmholtz Institut für Strahlen- und Kernphysik, Universität Bonn, Germany.

†Permanent address: Laboratory of Theoretical Physics, JINR Dubna, Moscow, Russia.

‡Electronic address: pedroni@pv.infn.it

§Present address: II. Physikalisches Institut, Universität Gießen, Germany.

are particularly sensitive to the behavior of the electromagnetic multipoles which are responsible for the excitation of the $D_{13}(1520)$ resonance. This feature can be understood from the multipole decomposition of the $\gamma N \to N\pi$ total cross section. In the following, we will use the so-called pion multipole notation, where E and M denote the electric or magnetic character of the incoming photon and the indices $l_\pm$ describe the coupling of the pion angular momentum l and the nucleon spin to the total angular momentum $J = l \pm 1/2$. Considering only partial waves with $l \leqslant 2$, the total unpolarized cross section σ can then be written as (see, for instance, [7])

$$\sigma \propto |E_{0+}|^2 + |M_{1-}|^2 + 6|E_{1+}|^2 + 2|M_{1+}|^2 + 6|M_{2-}|^2 + 2|E_{2-}|^2 + \cdots, \quad (1)$$

while the helicity dependent total cross section $\Delta\sigma_{31} = (\sigma_{3/2} - \sigma_{1/2})$, where the subscripts (1/2)3/2 correspond to the (anti)parallel γ-nucleon spin configuration, is

$$\Delta\sigma_{31} \propto -|E_{0+}|^2 - |M_{1-}|^2 - 3|E_{1+}|^2 + |M_{1+}|^2 - 6E^*_{1+}M_{1+} - 3|M_{2-}|^2 + |E_{2-}|^2 + 6E^*_{2-}M_{2-} + \cdots. \quad (2)$$

Since σ [see Eq. (1)] is given by the sum of separate contributions, only the few dominant partial waves can be evaluated reliably from unpolarized cross section data. On the other hand, the sensitivity to some selected weaker multipoles is greatly enhanced in $\Delta\sigma_{31}$ [Eq. (2)] as some of the terms change signs relative to others and new interference terms appear, e.g., between E_{2-} and M_{2-}, which are directly related to the $D_{13}(1520)$ excitation.

As an example, Fig. 1 illustrates the sensitivity to different resonances of (a) σ and (b) $\Delta\sigma_{31}$ for the $\gamma p \to n\pi^+$ reaction. In this figure, the predictions given by the MAID multipole analysis [5,6] (solution MAID03) are plotted as a function of the photon energy between 500 and 900 MeV. In both cases, the full curve represents the full MAID solution, while the dashed-dotted, dotted, and dashed curves represent calculations which differ only in that the coupling constants for the $D_{13}(1520)$, $S_{11}(1535)$, and $P_{11}(1440)$ resonances, respectively, have been artificially set to zero without a refit of the experimental data. The difference between the standard and modified solutions indicates the sensitivity of these observables to the different resonances.

As can be clearly seen from the comparison between Figs. 1(a) and 1(b), the influence of the $D_{13}(1520)$ resonance is greatly enhanced in the helicity dependent observable, while the sensitivity to $S_{11}(1535)$ is of opposite sign and less pronounced, and the sensitivity to $P_{11}(1440)$ is negligible for $E_\gamma \gtrsim 600$ MeV.

$\Delta\sigma_{31}$ is then well suited to extracting the helicity dependent amplitudes of the $D_{13}(1520)$ resonance, which are related to the multipole values as

$$A_{1/2} \propto \mathrm{Im}\left(3M^{(1/2)}_{2-} - E^{(1/2)}_{2-}\right),$$
$$A_{3/2} \propto \mathrm{Im}\left(M^{(1/2)}_{2-} + E^{(1/2)}_{2-}\right),$$

where the superscripts refer to the isospin, and the multipole values are at the resonance peak. The helicity dependent observables are in particular useful for evaluating the $A_{1/2}$ amplitude, which arises from the cancellation between electric and magnetic multipoles and which cannot be precisely evaluated using unpolarized data alone, since $\mathrm{Im}(M^{(1/2)}_{2-}) > \mathrm{Im}(E^{(1/2)}_{2-})$ and $|A_{1/2}| \ll |A_{3/2}|$ (see, for instance, [5]). An example of the sensitivity to this particular amplitude is given in Fig. 2, where three different predictions of the MAID analysis are shown for the unpolarized ($d\sigma/d\Omega$) and helicity

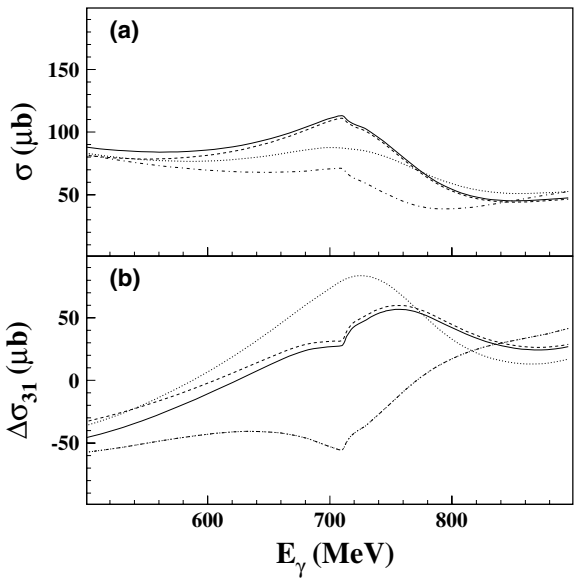

FIG. 1. Energy dependence of (a) unpolarized total cross section σ and (b) $\Delta\sigma_{31} = (\sigma_{3/2} - \sigma_{1/2})$ for the $\vec{\gamma}\vec{p} \to n\pi^+$ channel as described by the MAID analysis [5,6]. In both figures, the curves represent standard solution (full), no $D_{13}(1520)$ (dash-dotted), no $S_{11}(1535)$ (dotted), no $P_{11}(1440)$ (dashed).

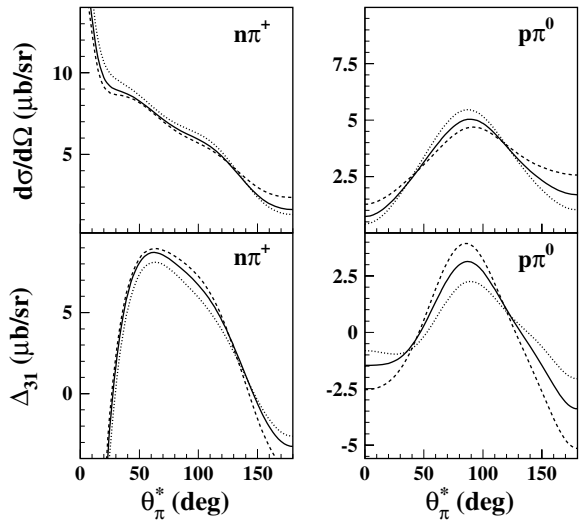

FIG. 2. Unpolarized (upper plots) and helicity dependent (lower plots) differential cross sections for the $\gamma p \to p\pi^0$ and $n\pi^+$ channels at $E_\gamma = 760$ MeV as predicted by three different versions of the MAID analysis: solid curve: $A_{1/2}(D_{13}(1520)) = -0.030$ GeV$^{-1/2}$ (standard MAID value); dashed curve: $A_{1/2} = 0$; dotted curve $A_{1/2}(D_{13}(1520)) = -0.060$ GeV$^{-1/2}$ (twice the standard MAID value).

dependent ($\Delta_{31} = d\sigma_{3/2}/d\Omega - d\sigma_{1/2}/d\Omega$) differential cross section of both $\gamma p \to N\pi$ channels at $E_\gamma = 760$ MeV [peak position of the $D_{13}(1520)$ resonance]. In all the plots of this figure, the solid curve represents the standard MAID solution ($A_{1/2} = -0.030$ GeV$^{-1/2}$), while the dashed curve represents the solution with $A_{1/2} = 0$ and the dotted curve is $A_{1/2} = -0.060$ GeV$^{-1/2}$, i.e., twice the standard MAID value.

Because of the reduced contribution given by the nonresonant π production mechanisms, $p\pi^0$ is more sensitive than $n\pi^+$ to $A_{1/2}$, and this sensitivity is greatly enhanced in Δ_{31}, mainly because of the last term of Eq. (2). For this reason, our first helicity dependent $p\pi^0$ data between 550 and 790 MeV [8] had already produced a significant change in the values of the E_{2-} and M_{2-} partial wave amplitudes with respect to the existing fits given by both the MAID and SAID [9] analyses.

However, to have a (quasi)model-independent determination of the properties of the $D_{13}(1520)$ resonance, different pion photoproduction channels need to be measured, also using different polarization observables. This will allow a reliable evaluation of both the isospin and the resonant and nonresonant components of all multipoles that play a non-negligible role in the second resonance region.

As a further step of this study, we present in this article the first measurement of the helicity dependent differential and total cross sections for the $\vec{\gamma}\vec{p} \to n\pi^+$ reaction from 450 to 790 MeV. With respect to the $p\pi^0$ case, the multipoles have a different isospin combination and some nonresonant partial waves, such as E_{0+}, play a more important role because the photon can directly couple to the π^+.

In Fig. 3, the different multipole contributions to σ for the $n\pi^+$ channel as predicted by MAID (solution MAID03) and SAID (solution FA04K) analyses are shown. While both analyses give similar values for the total unpolarized $n\pi^+$ cross section (continuous lines of Fig. 3), the predicted behavior of

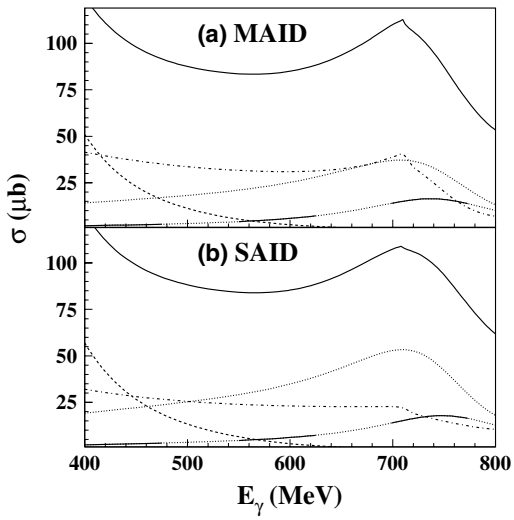

FIG. 3. Most important multipole contributions to the total unpolarized cross section for the $\gamma p \to n\pi^+$ reaction as predicted by (a) MAID [5,6] and (b) SAID [9] analyses. Continuous line: sum of all multipoles; dash-dotted line: contribution due to the E_{0+} multipole; dashed line: M_{1+} multipole; dotted line: E_{2-} multipole; continuous-dotted line: M_{2-} multipole.

the two main contributing multipoles (E_{0+} and E_{2-}) are very different. In the polarized case [see Eq. (2)], the negative sign of the E_{0+} contribution and the presence of the new interference term between the E_{2-} and M_{2-} multipoles highlights the differences between the two analyses.

Helicity dependent $n\pi^+$ data are then expected to have a big impact in the second resonance region where there are sizable uncertainties in the determination of the contributions given by the most important multipoles. The present data were obtained during the Gerasimov-Drell-Hearn (GDH) experiment at the Mainz Microtron (MAMI) [3,8,10–15], which studied the helicity structure of the exclusive and inclusive photoproduction cross sections and their contributions to the GDH sum rule.

II. EXPERIMENTAL SETUP

Only the main characteristics of the experimental setup are given here; more details may be found in Refs. [3,16]. The experiment was carried out at the Glasgow-Mainz tagged photon facility of the MAMI accelerator in Mainz [17,18]. Circularly polarized photons are produced by bremsstrahlung of longitudinally polarized electrons. A strained GaAs photocathode routinely delivered electrons with a degree of polarization of about 75% [19]. The electron polarization was monitored with a precision of 3% by means of a Moeller polarimeter. The photon polarization was evaluated according to Ref. [20]. The photon energy was determined by the tagging spectrometer which has an energy resolution of about 2 MeV. The tagging efficiency was continuously monitored with a precision of 2% during the data-taking by an e^+e^- pair spectrometer installed downstream of the main hadron detector, and absolute values were measured periodically using a 100% efficient lead glass detector.

A butanol (C_4H_9OH), frozen-spin target [21] provided the polarized protons. The system consisted of a horizontal dilution refrigerator and a superconducting magnet ($\cong$2.5 T), used in the polarization phase, together with a microwave system for dynamic nuclear polarization. During the measurement, the polarization was maintained in the frozen-spin mode at a temperature of about 50 mK and a magnetic field of 0.4 T, supplied by a small superconducting holding coil inside the cryostat. The proton polarization was measured using NMR techniques with a precision of 1.6%. Polarization values higher than 80% and relaxation times in the frozen-spin mode of about 200 h were regularly achieved.

Photoemitted hadrons were registered in the large acceptance detector DAPHNE [22] (see Fig. 4), which is a charged-particle tracking detector covering the full azimuthal angular region and polar angles $\theta_{\rm lab}$ from 21° to 159°. It

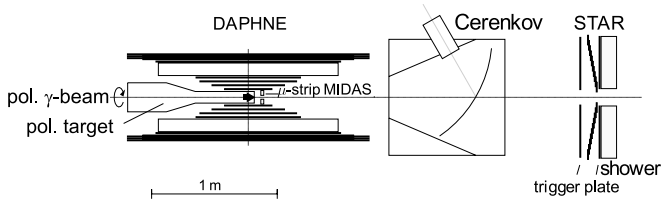

FIG. 4. Schematic side view of the GDH detector at MAMI.

consists of three cylindrical multiwire proportional chambers, surrounded by segmented plastic scintillator layers and by a scintillator-absorber sandwich that allows the detection of neutral pions with an efficiency of about 20%.

In addition to DAPHNE, Fig. 4 shows forward detector components, the silicon microstrip detector array system (MIDAS) [23], an aerogel Cerenkov counter to suppress electromagnetic background, and the annular ring detector Scintillators from Tübingen for Angle Reconstruction (STAR) [24] followed by a forward scintillator-lead sandwich counter. The particle identification capabilities of MIDAS and STAR were insufficient to ensure reliable separation of π^+ from $e^\pm$ and relativistic protons, and thus they were not used in the present analysis.

III. DATA ANALYSIS

The data analysis of the $\vec{\gamma}\,\vec{p} \to n\pi^+$ process was performed in two parts. In the first stage, the analysis method was developed and verified using calibration data taken with an unpolarized photon beam and a pure liquid hydrogen target. In the second part, the same method was used with the polarized data. A detailed discussion of the overall analysis can also be found in Ref. [3], where the helicity dependent $n\pi^+$ data are shown from $E_\gamma = 180$ MeV to $E_\gamma = 450$ MeV, and in Ref. [16].

A. Unpolarized data

As in Ref. [3], events with a single charged track recognized as a pion were selected in order to identify the $n\pi^+$ channel. The charged pions were identified using a combination of the ΔE-E technique described in [12] and the range method described in [25]. The range method uses the charged-particle energy losses in all traversed DAPHNE scintillator layers to discriminate between protons and charged pions (with a systematic misidentification error of 2%) and to determine their kinetic energy.

However, this procedure can only be used for particles that are stopped in the detector. The identification of charged pions that escape the detector (without the determination of their kinetic energy) is performed by comparing information provided by the geometrical path of the particle inside the detector with the energy deposited in the thickest scintillator layer, which has the best energy resolution [12]. This technique cannot distinguish charged pions from quasirelativistic protons having a momentum higher than $\simeq$900 MeV/c.

The background contributions to the $n\pi^+$ channel which remain after this procedure come from the $n\pi^+\pi^0$, $p\pi^+\pi^-$, $p\pi^0$, and $p\eta \to p\pi^+\pi^-\pi^0$ final states (see Fig. 5), and methods to identify and correct for this background are described as follows:

(i) The $n\pi^+\pi^0$ channel is the major source of background. About 50% of this contribution can be removed event-by-event when one or two neutral particles, identified as photons, are detected in coincidence [12]. The contribution of the remainder to the $n\pi^+$ yield was evaluated, for each photon energy interval, starting from the experimental angular distributions of events having a charged pion in coincidence with two detected photons ($N^{\gamma\gamma}_{\pi^+}$). These events are surely coming from the $n\pi^+\pi^0$ channel, since the contribution given by the $N\pi\pi\pi$ processes can be neglected within the measured photon energy range. These angular distributions were then multiplied with the simulated ratio $N^{\gamma\gamma}_{\pi^+}/N_{\pi^+}$ (where N_{π^+} represents the yield of events without any accompanying neutral track) and subtracted from the experimental N_{π^+} yield. This ratio was obtained from a GEANT-based program which models accurately the geometry and composition of the GDH detector setup.

An example of the background angular distributions that were thus obtained is shown in Fig. 5. The background contribution is plotted as a function of the pion angle in the center-of-mass system of the $n\pi^+$ channel (θ^*_π) and at $E_\gamma = 743 \pm 10$ MeV, where the $n\pi^+\pi^0$ background reaches its maximum. The measured N_{π^+} yield is given by open circles, while the evaluated background contribution from the $n\pi^+\pi^0$ channel is shown by the filled squares. This background is negligible at $E_\gamma \sim 460$ MeV and increases smoothly to $\simeq$20% of the overall measured N_{π^+} yield at 750 MeV. Taking into account the good confidence in the simulated efficiencies for the $n\pi^+\pi^0$ process [12], the systematic error in the background is estimated to be 10%.

(ii) The $p\pi^+\pi^-$ reaction also produces a significant background contribution when only one charged pion is emitted inside the DAPHNE acceptance. This background was evaluated, assuming a uniform phase space distribution, with a simulation which incorporates the experimental

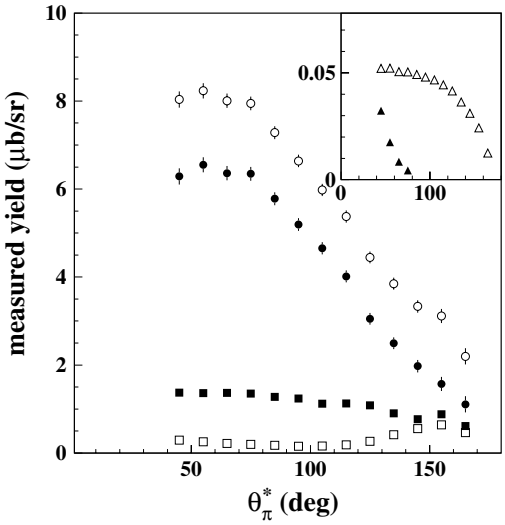

FIG. 5. Different background contributions to the $n\pi^+$ channel at $E_\gamma = 743 \pm 10$ MeV as a function of the pion angle in the center-of-mass system θ^*_π for data taken with unpolarized photons and unpolarized target. Open circles: measured yield of the selected N_{π^+} events; filled squares: background contribution from the $n\pi^+\pi^0$ channel; open squares: background contribution from the $p\pi^+\pi^-$ channel; open triangles: background contribution from the $p\pi^0$ channel; filled triangles: background contribution from the $p\eta$ channel; filled circles: obtained yield after subtraction of all background contributions. The errors shown are statistical only.

total cross section values for the $p\pi^+\pi^-$ channel that had been measured with the same apparatus [26,27]. The resulting contribution was found to be at most $\simeq$6% of the measured $n\pi^+$ yield at 780 MeV; its angular behavior is shown in Fig. 5 (open squares) at $E_\gamma = 743 \pm 10$ MeV.

(iii) The $p\pi^0$ channel produces background if a high-momentum recoil proton is misidentified as a charged pion. This contribution was evaluated using the angular distributions given by the SAID (solution FA04K) analysis [9] and found to be at most $\simeq$0.2% of the overall measured $n\pi^+$ yield at 780 MeV. Its angular behavior is shown in Fig. 5 (filled triangles) at $E_\gamma = 743 \pm 10$ MeV.

(iv) The $\gamma p \to p\eta \to p\pi^+\pi^-\pi^0$ process produces background when, among all photoemitted particles, only one charged pion is emitted inside the DAPHNE acceptance. This contribution was evaluated using the evaluated $p\eta$ angular distributions measured with the two-arms photon spectrometer (TAPS) detector [28] and was found to be at most $\simeq$0.5% of the measured $n\pi^+$ yield at 750 MeV. Its angular behavior is shown in Fig. 5 (filled triangles) at $E_\gamma = 743 \pm 10$ MeV.

A relative systematic error of 10% is also estimated for the background contributions from the last three channels. The addition in quadrature of all different systematic contributions gives an overall systematic error of about 4% of $d\sigma/d\Omega$ for $\theta_\pi^* \leqslant 80^\circ$, which increases linearly up to $\sim$10% of $d\sigma/d\Omega$ at $\theta_\pi^* = 155^\circ$.

The resulting unpolarized differential cross sections for $\gamma p \to n\pi^+$ in the energy range $463 < E_\gamma < 783$ MeV are shown in Figs. 6 and 7 as a function of θ_π^* [16]. These data

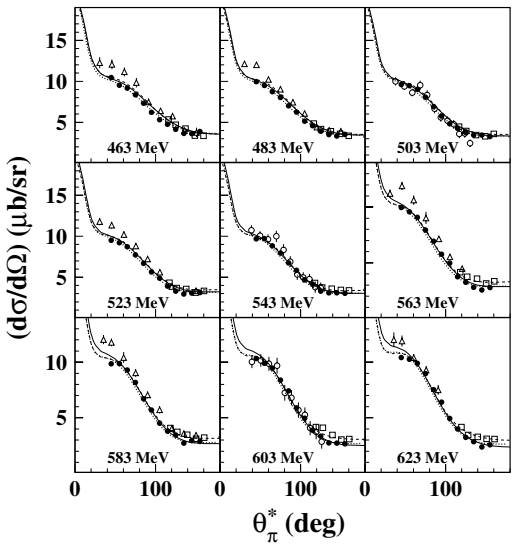

FIG. 6. Measured unpolarized differential cross section for the $\gamma p \to n\pi^+$ reaction for photon energies from 463 to 623 MeV (filled circles) compared with previous experimental data and with MAID [5,6] (solid lines) and SAID [9] (dashed lines) analyses. Open triangles: [29]; open circles: [30]; open squares: [31]. The dotted curve represents our modified MAID solution (see text). The errors shown are statistical only.

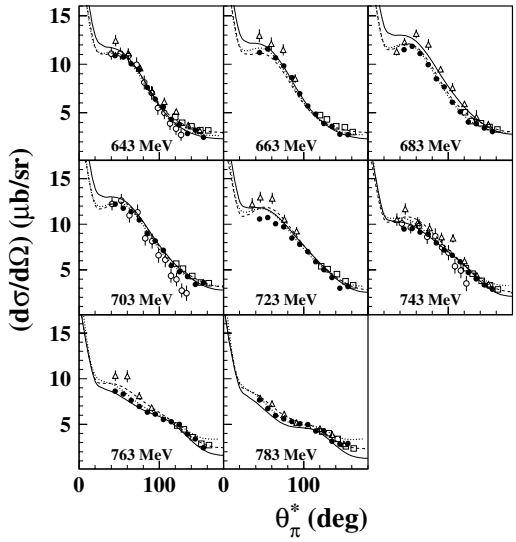

FIG. 7. As in Fig. 6, but for photon energies from 643 to 783 MeV.

are compared with the most recent available data sets, from Tokyo [29] and Bonn [30,31], and with the results of MAID (solution MAID03) [5,6] and SAID (solution FA04K) [9], which represent, at the moment, the most comprehensive multipole analyses of the existing $N\pi$ database.

The general good agreement with predictions of multipole analyses and the two data sets from Bonn [30,31], which are the most accurate measurements performed up to now, shows that the detector response and the background subtraction method are well under control.

Using the present data, the total unpolarized cross section for the $\gamma p \to n\pi^+$ channel was also derived. The extrapolation into the unobserved forward and backward angle regions was made using the MAID analysis. The values of the extrapolation correction were found to be at most $\simeq$15% of the measured yield. A very similar correction was found when using the SAID analysis.

To evaluate the systematic error associated with this procedure, a different extrapolation algorithm has been used. The correction for the unobserved forward (backward) polar region was made assuming the same behavior for $d\sigma/d\Omega$ as the one observed by previous experiments [31–33], e.g., a linear increase (constant behavior) at very forward (backward) angles. The maximum relative difference between these two extrapolation corrections was found to be $\simeq$20%, which gives an estimate of the systematic error of the extrapolation. This gives an overall systematic error on the measured total cross section of $\sim \pm 5\,\mu$b.

In Fig. 8, the total cross section thus obtained is again compared with the SAID [9] and MAID [5,6] multipole analysis results. The same figure shows our results previously obtained at $E_\gamma \leqslant 450$ MeV [3]. No other data are available for this observable. The present experimental data agree with both theoretical analyses at $E_\gamma > 450$ MeV within the quoted statistical and systematic errors. This new unpolarized data set considerably improves the existing database above 450 MeV.

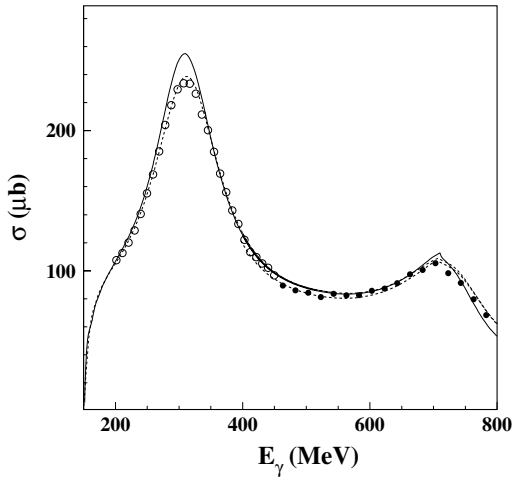

FIG. 8. Unpolarized total cross section data for $\gamma p \to n\pi^+$ (filled circles) are compared with our previous results at $E_\gamma \leqslant 450$ MeV [3] (open circles) and with the MAID [5,6] (solid line) and SAID [9] (dashed line) analyses. The dotted curve for $E_\gamma \geqslant 400$ MeV represents our modified MAID solution (see text). Only statistical errors are shown.

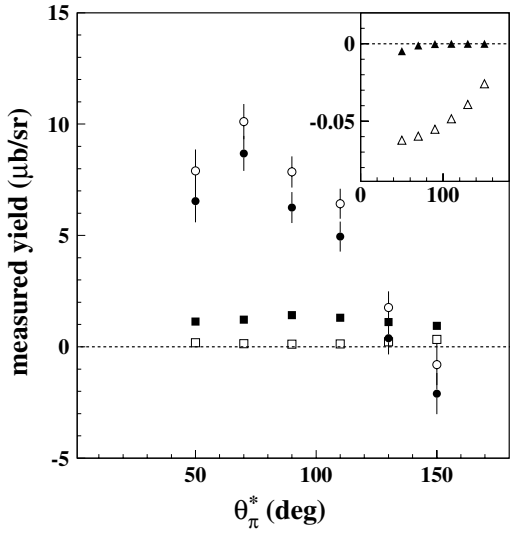

FIG. 9. Different background contributions to the $n\pi^+$ channel at $E_\gamma = 743 \pm 10$ MeV as a function of the pion angle in the center-of-mass system (θ^*_π). Open circles: measured yield of the selected N_{π^+} events; filled squares: background contribution from the $n\pi^+\pi^0$ channel; open squares: background contribution from the $p\pi^+\pi^-$ channel; open triangles: background contribution from the $p\pi^0$ channel; filled triangles: background contribution from the $p\eta$ channel; filled circles: obtained yield after subtraction of all background contributions. Only statistical errors are shown.

B. Polarized data

The same analysis method is applied to the doubly polarized data to obtain the difference between the helicity cross sections $\sigma_{1/2}$ and $\sigma_{3/2}$. The difference is taken to cancel the background from the unpolarized carbon and oxygen nuclei in the butanol target [10].

The background from the polarized $n\pi^+\pi^0$ reaction was evaluated using a procedure similar to item (1) of Sec. III A. An example of the angular distributions that were thus obtained is shown in Fig. 9 as a function of θ^*_π at $E_\gamma = 743 \pm 10$ MeV. The measured $\Delta N_{\pi^+} = N^{3/2}_{\pi^+} - N^{1/2}_{\pi^+}$ yield is given by open circles, while the evaluated background contribution from the $n\pi^+\pi^0$ channel is shown by the filled squares. This background is negligible up to $E_\gamma \sim 500$ MeV and increases smoothly to $\simeq$15% of the overall measured ΔN_{π^+} yield at 750 MeV.

For the evaluation of the background coming from the $p\pi^+\pi^-$ reaction, our polarized data have been used [26,27]. The resulting contribution was found to be at most $\simeq$25% of the measured ΔN^+_π yield at $E_\gamma \sim 600$ MeV; its angular behavior is shown in Fig. 9 (open squares) at $E_\gamma = 743 \pm 10$ MeV.

The background from the polarized $p\pi^0$ reaction was again simulated using the SAID analysis, which well reproduces the polarized $p\pi^0$ angular distributions previously measured by our Collaboration [8] in the second resonance region (shown later in Fig. 15). The absolute value of this contribution was found to be at most $\simeq$0.1% of the measured ΔN^+_π yield at $\sim$780 MeV; its angular behavior is shown in Fig. 9 (filled triangles) at $E_\gamma = 743 \pm 10$ MeV.

Finally, in evaluating the $p\eta$ background contribution, a helicity asymmetry $(\sigma_{1/2} - \sigma_{3/2})/(\sigma_{1/2} + \sigma_{3/2}) = -0.97$ was assumed for the $p\eta$ channel following the calculation of Refs. [5,6]. This assumption is consistent with some of our previous experimental results [13]. The absolute value of this contribution was found to be at most $\simeq$0.25% of the measured $n\pi^+$ yield at $\sim$750 MeV; its angular behavior is shown in Fig. 5 (filled triangles) for $E_\gamma = 743 \pm 10$ MeV.

A relative systematic error of 10% is again assumed for all evaluated background contributions.

IV. RESULTS AND DISCUSSIONS

A. Polarized cross sections

In Figs. 10 and 11 we present the obtained helicity dependent differential cross section $\Delta_{31} = (d\sigma/d\Omega)_{3/2} - (d\sigma/d\Omega)_{1/2}$ for the $n\pi^+$ channel from 463 to 783 MeV and compare these data with the previously mentioned analyses. These are the first published data for this observable.

All errors shown are statistical only. The addition in quadrature of all the different sources of systematic errors gives an overall systematic error of about 5.5% of Δ_{31} for $\theta^*_\pi \leqslant 80^\circ$, which increases linearly up to about 11% of Δ_{31} at $\theta^*_\pi = 150^\circ$.

The total polarized cross section $\Delta\sigma_{31} = (\sigma_{3/2} - \sigma_{1/2})$ was also evaluated from these data. The extrapolation into the unobserved region was made using the MAID calculation, which reproduces the measured differential cross sections better than SAID. This correction has a value of about $-18\,\mu$b at $E_\gamma = 460$ MeV and rises smoothly to about $-5\,\mu$b at $E_\gamma = 780$ MeV.

To evaluate the systematic error associated with this procedure, other extrapolation algorithms have been used. In a first method, the SAID model was used to evaluate this correction. With a different and more elaborate procedure,

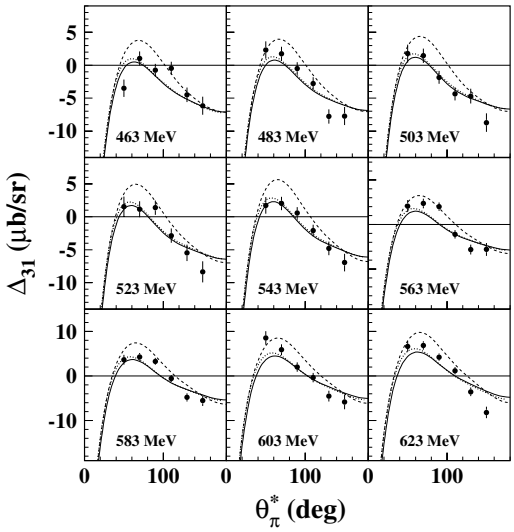

FIG. 10. Measured polarized differential cross section $\Delta_{31} = (d\sigma/d\Omega)_{3/2} - (d\sigma/d\Omega)_{1/2}$ for the $\vec{\gamma}\vec{p} \to n\pi^+$ reaction for photon energies from 463 to 623 MeV (filled circles) compared with theoretical predictions. Curves as in the previous figures. Only statistical errors are shown.

the separate evaluation of $(d\sigma/d\Omega)_{3/2}$ and $(d\sigma/d\Omega)_{1/2}$ was carried out from the combination of the measured data sets for $(d\sigma/d\Omega)$ and Δ_{31}. A separate extrapolation procedure was then performed for each helicity case, and the difference between the two extrapolation corrections was evaluated. A linear behavior for both helicity dependent differential cross sections outside the measured angular range was assumed during this procedure. The values at the two extreme θ_π^* values were taken as $(d\sigma/d\Omega)_{3/2}(0^\circ, 180^\circ) = 0$ and $(d\sigma/d\Omega)_{1/2}(0^\circ, 180^\circ) = 2(d\sigma/d\Omega)(0^\circ, 180^\circ)$. The values of $d\sigma/d\Omega$ were taken from previous experiments [31–33].

The maximum relative discrepancy between all different extrapolation methods was found to be $\simeq$20%. This value is assumed to be the systematic error of the extrapolation. This gives an overall systematic error of $\sim\pm 6\,\mu$b for $\Delta\sigma_{31}$.

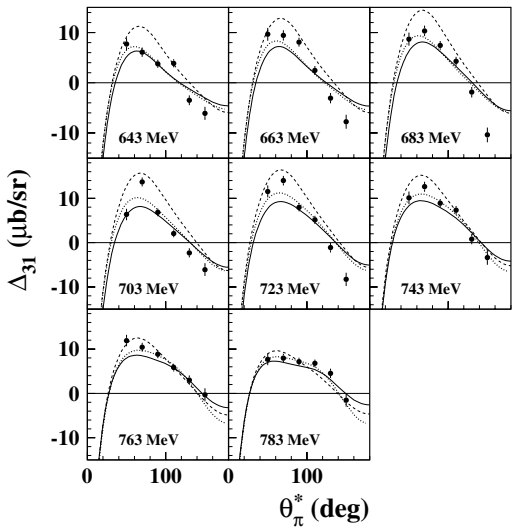

FIG. 11. As in Fig. 10, but for photon energies from 643 to 783 MeV.

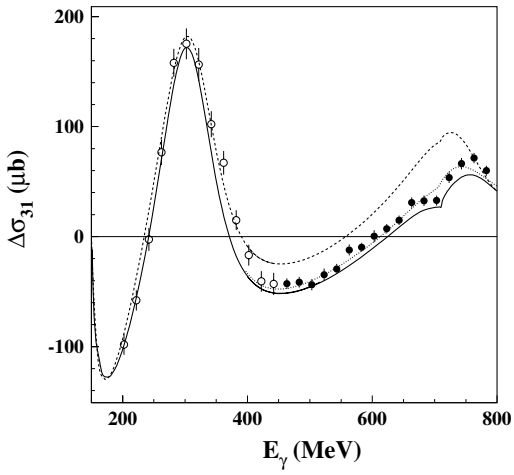

FIG. 12. Polarized total cross section for $\gamma p \to n\pi^+$ compared with the analyses of MAID [5,6] (solid line) and SAID [9] (dashed line) and our previous data at $E_\gamma \leqslant 450$ MeV [3] (open circles). The dotted curve for $E_\gamma \geqslant 400$ MeV represents our modified MAID solution (see text).

In Fig. 12, the evaluated helicity dependent total cross section $\Delta\sigma_{31} = (\sigma_{3/2} - \sigma_{1/2})$ is shown together with our previous polarized data at $E_\gamma \leqslant 450$ MeV [3] and compared with the SAID and MAID analyses. In contrast to the unpolarized case, there is now a clear systematic discrepancy between the prediction of SAID and that of MAID at $E_\gamma \gtrsim 450$ MeV, with our data being in general closer to the latter prediction. The reason for the discrepancy between the models can be traced down to the different predicted contributions of the most relevant multipoles for the $\gamma p \to n\pi^+$ channel, as shown in Figs. 3 and 14.

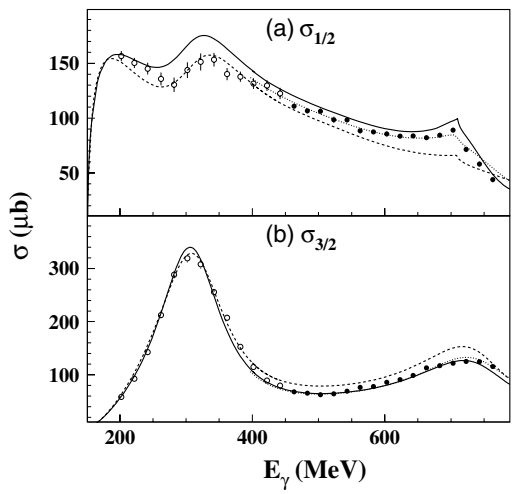

FIG. 13. Helicity dependent cross sections $\sigma_{1/2}$ (a) and $\sigma_{3/2}$ (b) for the $\vec{\gamma}\vec{p} \to n\pi^+$ reaction (filled circles), combined with our previous data at $E_\gamma \leqslant 450$ MeV [3] (open circles), compared with model predictions. Curves as in the previous figure. Only statistical errors are shown.

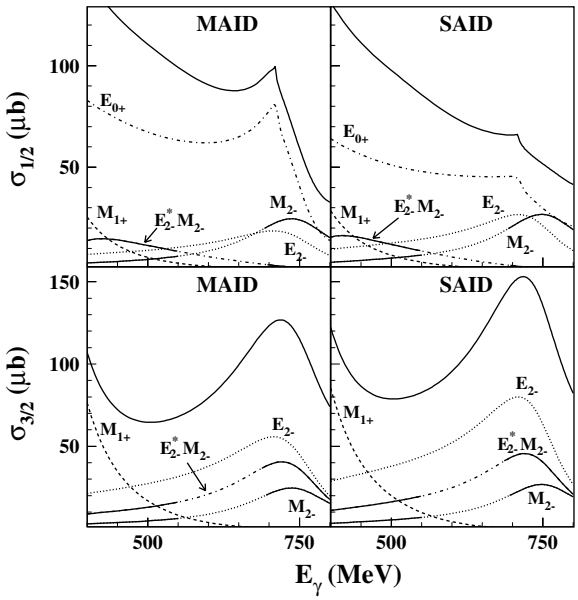

FIG. 14. Main multipole contributions to the helicity dependent total cross sections $\sigma_{1/2}$ (upper) and $\sigma_{3/2}$ (lower) for the $\gamma p \to n\pi^+$ reaction as predicted by the MAID [5,6] and SAID [9] analyses. Continuous line: sum of all multipoles; dash-dotted line: contribution due to E_{0+} multipole; dashed line: M_{1+} multipole; dotted line: E_{2-} multipole; continuous-dotted line: M_{2-} multipole; continuous-dash-dotted line: $E_{2-}^{*}M_{2-}$ interference term.

A deeper insight into the contribution of the different multipoles can be obtained from the separate helicity dependent total cross sections $\sigma_{1/2}$ and $\sigma_{3/2}$ that can be deduced from the measured unpolarized and polarized total cross sections. The results of this separation are shown in Figs. 13(a) and 13(b) for $\sigma_{1/2}$ and $\sigma_{3/2}$, respectively. In these figures, the model predictions from SAID and MAID are also shown together with the same observables evaluated from our previously published results at $E_\gamma \leqslant 450$ MeV [3].

In Fig. 14 the main multipole contributions as predicted by MAID and SAID analyses are shown for both the $\sigma_{1/2}$ and the $\sigma_{3/2}$ case. As can be clearly seen from Fig. 14, the $\sigma_{1/2}$ cross section at $E_\gamma \gtrsim 400$ MeV is mainly sensitive to the behavior of the E_{0+} multipole. This partial wave is responsible for the clear cusp structure seen in Fig. 13(a) at $E_\gamma \sim 705$ MeV. Such a feature, which had already been seen experimentally in the same photon energy region for $(d\sigma/d\Omega)$ at the most backward angles [31,34,35] is due to the onset of the η production mechanism which takes place at $E_\gamma = 707.7$ MeV. The strong intermediate excitation of the $S_{11}(1535)$ resonance which is responsible for this reaction causes, by unitarity, a sizable change in the behavior of the $n\pi^+$ channel. The discrepancy between MAID and SAID is mainly due to the predicted behavior of the E_{0+} multipole (see Fig. 14).

On the other hand, the behavior of $\sigma_{3/2}$ in the second resonance region [Fig. 13(b)] clearly shows a resonant structure essentially due to excitation of the $D_{13}(1520)$ state. In this case, the E_{2-} multipole gives the most relevant contribution, and its role is enhanced because of the presence of an interference with the M_{2-} multipole (see Fig. 14). In this case, the discrepancy between MAID and SAID is mainly due to the E_{2-} multipole. A closer inspection of the predicted behavior of E_{0+} and E_{2-} multipoles revealed that in both cases, the discrepancy lies in the real part of the multipoles. Unlike the imaginary parts, the real parts of the multipoles have a stronger model dependence because of the meson loop contributions and coupled channel effects.

B. Partial wave analysis

To extract more precise information about the $D_{13}(1520)$ and $S_{11}(1535)$ resonances, a fit of all our polarized and unpolarized $N\pi$ differential cross sections measured from 400 to 800 MeV has been performed based on a modified MAID analysis. The present measurement together with our previous polarized and unpolarized measurements for the $p\pi^0$ [8] and $n\pi^+$ [3] channels have been used. This database contains 574 points in total.

Within the MAID framework, 12 free parameters were used in our fit which correspond to the couplings of the resonances that can play a sizable role in the photon energy range covered by the database, i.e., $P_{33}(1232)$, $P_{11}(1440)$, $D_{13}(1520)$, $S_{11}(1535)$, $S_{31}(1620)$, $S_{11}(1650)$, $D_{33}(1700)$, and $F_{15}(1680)$. The widths, masses, and single pion branching ratios of all resonances were taken from the Particle Data Group (PDG) [36]. The pseudo-scalar/pseudo-vector (PS/PV) mixing parameter, which describes the Born term contribution and mainly affects the $E_{0+}^{1/2}$ and $M_{1-}^{1/2}$ amplitudes, was taken from the standard MAID solution. Only the experimental statistical errors were taken into account in the procedure; the overall reduced χ^2 of the fit is 2.6.

This modified MAID solution is shown by the dotted curves in Figs. 6–8 and 10–13. The comparison of this solution with some of our published helicity dependent $p\pi^0$ data is also shown in Fig. 15. Our fit, with respect to the standard MAID solution, produced a significant change, within the measured photon energy range, only for the E_{0+}, M_{1-}, and E_{2-} multipoles.

The transition from the multipole representation to the helicity amplitudes requires a separation of resonant and nonresonant contributions of a given partial wave and is therefore model dependent. Once this separation is done, the standard procedure described in Ref. [37] can be used. Since the D_{13} partial wave amplitudes are almost purely imaginary at the resonance position, in this case the model dependence is weak. This is different for the S_{11} partial wave, where the phase at the resonance position is essentially different from 90° and the nonresonant background leads to contributions in both real and imaginary parts. Our numerical values for these two resonances are shown in Table I together with the PDG latest estimate [36].

To evaluate the systematic error associated with the uncertainties on all the resonance parameters that were used, the fitting procedure was repeated several times with different sets of parameters randomly selected in an uniform way within the uncertainties given by the PDG. The uncertainties related to the Born terms were evaluated by additionally including the (PS/PV) mixing parameter inside the fitting procedure.

TABLE I. S_{11} and D_{13} helicity amplitudes $A_{1/2}$ and $A_{3/2}$ for the proton (in units of $\mathrm{GeV}^{-1/2}$) estimated from our analysis based on the MAID parametrization (denoted as Modified MAID). The numbers are compared with the standard MAID (MAID03) solution, SAID analysis [9], and PDG [36], see text. The first error stems from the fitting procedure; the second one is the estimated systematic error ($\pm\delta/2$) arising from the uncertainties in the resonance parameters, see text.

Solution	$A_{1/2}(S_{11})$	$A_{1/2}(D_{13})$	$A_{3/2}(D_{13})$
MAID03	0.073	−0.030	0.166
SAID	0.030 ± 0.003	-0.024 ± 0.002	0.135 ± 0.002
PDG	0.090 ± 0.030	-0.024 ± 0.009	0.166 ± 0.005
Modified MAID	$0.079 \pm 0.003 \pm 0.011$	$-0.039 \pm 0.005 \pm 0.009$	$0.168 \pm 0.002 \pm 0.007$

The difference δ between the minimum and maximum values of the helicity amplitudes of the $D_{13}(1520)$ and $S_{11}(1535)$ resonances that were thus evaluated is our estimation of the systematic error associated with the fitting procedure, which is given (as $\pm\delta/2$) in Table I.

For the S_{11} resonance, we find a small increase in the $A_{1/2}$ helicity amplitude with respect to the standard MAID result. Our value of 0.079 ± 0.003 $\mathrm{GeV}^{-1/2}$ is still about 20% smaller than values obtained from η photoproduction analyses in the range of $0.100 - 0.120$ $\mathrm{GeV}^{-1/2}$ [38] but is considerably larger than the SAID [9] value. However, in a reanalysis [39], the SAID group also obtains values in the range of our fit.

For the D_{13} we obtain similar values as in our previous analysis [8], where only the polarized $p\pi^0$ data had been analyzed. With the π^0 data alone, we obtained the values of -0.038 ± 0.003 and 0.147 ± 0.010 $\mathrm{GeV}^{-1/2}$ for the $A_{1/2}$ and $A_{3/2}$ amplitudes, respectively. Our new fit, which includes additional and more precise double polarization data measured over a wider angular range, supports the larger value of $A_{1/2}$ compared with PDG and finds a more stable value for the $A_{3/2}$ amplitude of 0.168 ± 0.002 $\mathrm{GeV}^{-1/2}$, in very good agreement with PDG.

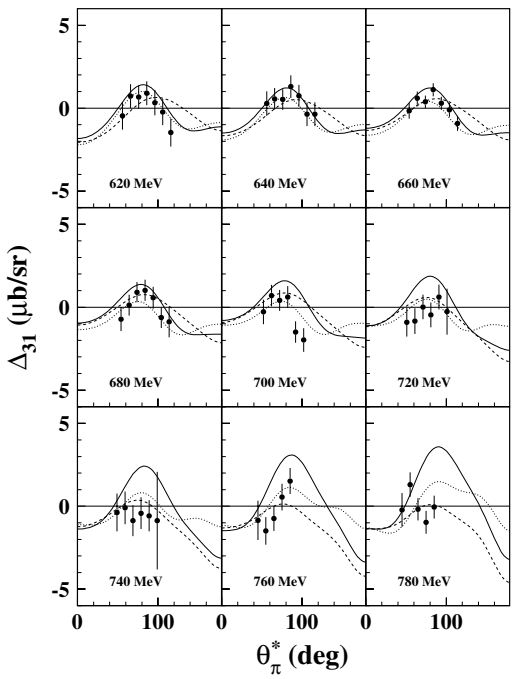

FIG. 15. Our previously measured polarized differential cross sections $\Delta\sigma_{31} = (\sigma_{3/2} - \sigma_{1/2})$ for the $\vec{\gamma}\vec{p} \to p\pi^0$ channel put from 620 to 780 MeV compared with the MAID (solid lines) and SAID analyses (dashed lines) and to the results of our fit (dotted lines).

V. CONCLUSIONS

Both the unpolarized and the helicity dependent total and differential cross sections for the $\gamma p \to n\pi^+$ channel have been measured in the photon energy interval 450–790 MeV. While the unpolarized data are in good agreement with the existing MAID and SAID multipole analyses, our helicity dependent results, the first of their kind, highlight the differences between the two models caused by their enhanced sensitivity to the main multipoles contributing to this channel.

Although the $n\pi^+$ channel is mainly produced from an intermediate excitation of the $D_{13}(1520)$ resonance, a pronounced cusp structure is clearly observed at about 700 MeV in the $\sigma_{1/2}$ cross section. This feature is due to the onset of the η production process.

These data provide a strong constraint for a precise determination of the partial waves playing a role in the second resonance region and of the parameters of the $D_{13}(1520)$ and $S_{11}(1535)$ resonances. From a partial wave fit of these and our previous $N\pi$ results from 400 to 800 MeV, we have determined the photocoupling parameters of the $D_{13}(1520)$ and $S_{11}(1535)$ resonances. The obtained results imply that $A_{1/2}$ for the $D_{13}(1520)$ resonance is larger (in absolute value) by about 60% than the standard PDG values, while $A_{1/2}$ for the $S_{11}(1535)$ resonance is about 20% smaller than the values obtained from η photoproduction analyses.

To reduce the sizable systematic uncertainties that still affect these evaluations, new experiments are in preparation at the new MAMI-C facility in Mainz that will extend the measurement of the $N\pi$ channels to cover almost the full angular range up to photon beam energies of ∼1.4 GeV with the possibility of accessing additional polarization observables.

ACKNOWLEDGMENTS

The authors wish to acknowledge the excellent support of the accelerator group of MAMI. This work was supported by the Deutsche Forschungsgemeinschaft (SFB 201, SFB 443,

and Schwerpunktprogramm), INFN–Italy, FWO Vlaanderen–Belgium, IWT–Belgium, U.K. Engineering and Physical Science Council, DAAD, Russian Foundation for Basic Research (RFBR 05-02-16810), and Grant-in-Aid, Monbusho (Japan).

[1] R. Beck *et al*., Phys. Rev. Lett. **78**, 606 (1997).
[2] R. Beck *et al*., Phys. Rev. C **61**, 035204 (2000).
[3] J. Ahrens *et al*., Eur. Phys. J. A **21**, 323 (2004).
[4] G. Blanpied *et al*., Phys. Rev. C **64**, 025203 (2001).
[5] D. Drechsel, O. Hanstein, S. S. Kamalov, and L. Tiator, Nucl. Phys. **A645**, 145 (1999), http://www.kph.uni-mainz.de/MAID/.
[6] D. Drechsel, S. S. Kamalov, and L. Tiator, Phys. Rev. D **63**, 114010 (2001).
[7] D. Drechsel, Prog. Part. Nucl. Phys. **34**, 181 (1995).
[8] J. Ahrens *et al*., Phys. Rev. Lett. **88**, 232002 (2002).
[9] R. A. Arndt, W. J. Briscoe, I. I. Strakovsky, and R. L. Workman, Phys. Rev. C **66**, 055213 (2002), http://www.gwdac.phys.gwu.edu/.
[10] J. Ahrens *et al*., Phys. Rev. Lett. **84**, 5950 (2000).
[11] J. Ahrens *et al*., Phys. Rev. Lett. **87**, 022003 (2001).
[12] J. Ahrens *et al*., Phys. Lett. **B551**, 49 (2003).
[13] J. Ahrens *et al*., Eur. Phys. J. A **17**, 241 (2003).
[14] J. Ahrens *et al*., Phys. Lett. **B624**, 173 (2005).
[15] J. Ahrens *et al*., Eur. Phys. J. A **26**, 135 (2005).
[16] T. Rostomyan, Ph.D. thesis, University of Gent, 2005.
[17] G. Anthony, J. Kellie, S. Hall, G. Miller, and J. Ahrens, Nucl. Instrum. Methods A **301**, 230 (1991).
[18] S. Hall, G. Miller, R. Beck, and P. Jennewein, Nucl. Instrum. Methods A **368**, 698 (1996).
[19] K. Aulenbacher, Nucl. Instrum. Methods A **391**, 498 (1997).
[20] H. Olsen and L. Maximon, Phys. Rev. **114**, 887 (1959).
[21] C. Bradtke *et al*., Nucl. Instrum. Methods A **436**, 430 (1999).
[22] G. Audit *et al*., Nucl. Instrum. Methods A **301**, 473 (1991).
[23] S. Altieri *et al*., Nucl. Instrum. Methods A **452**, 185 (2000).
[24] M. Sauer, A. Fuchs, P. Grabmayr, and J. Leypoldt, Nucl. Instrum. Methods A **378**, 146 (1996).
[25] A. Braghieri *et al*., Nucl. Instrum. Methods A **343**, 623 (1994).
[26] M. Lang, Ph.D. thesis, University of Mainz, 2004.
[27] H. Holvoet, Ph.D. thesis, University of Gent, 2001.
[28] B. Krusche *et al*., Phys. Rev. Lett. **74**, 3736 (1995).
[29] H. Fujii, T. Kondo, F. Takasaki, S. Yamada, S. Homma, K. Huke, S. Kato, H. Okuno, I. Endo, and H. Fujii, Nucl. Phys. **B120**, 395 (1977).
[30] K. Buechler *et al*., Nucl. Phys. **A570**, 580 (1994).
[31] H. Dannhausen, E. Durwen, H. Fischer, M. Leneke, W. Niehaus, and F. Takasaki, Eur. Phys. J. A **11**, 441 (2001).
[32] S. Ecklund and R. Walker, Phys. Rev. **159**, 1195 (1967).
[33] C. Betourne, J. Bizot, J. Perez-y Jorba, J. Treille, and W. Schmidt, Phys. Rev. **172**, 1343 (1968).
[34] L. Hand and C. Schaerf, Phys. Rev. Lett. **6**, 229 (1961).
[35] K. H. Althoff, M. Gies, O. Kaul, K. Konigsmann, D. Menze, W. Meyer, T. Miczaika, W. Pfeil, E. Roderburg, and W. Schwille, Z. Phys. C **1**, 327 (1979).
[36] S. Eidelman *et al*., Phys. Lett. **B592**, 1 (2004).
[37] R. A. Arndt, R. L. Workman, Z. Li, and L. D. Roper, Phys. Rev. C **42**, 1864 (1990).
[38] B. Krusche and S. Schadmand, Prog. Part. Nucl. Phys. **51**, 399 (2003).
[39] R. L. Workman (private communication).